Grain Boundary Engineering for Structure Materials of Nuclear Reactors

L. Tan, T.R. Allen, J.T. Busby

PII: S0022-3115(13)00553-9
DOI: http://dx.doi.org/10.1016/j.jnucmat.2013.03.050
Reference: NUMA 47318

To appear in: *Journal of Nuclear Materials*

Please cite this article as: L. Tan, T.R. Allen, J.T. Busby, Grain Boundary Engineering for Structure Materials of Nuclear Reactors, *Journal of Nuclear Materials* (2013), doi: http://dx.doi.org/10.1016/j.jnucmat.2013.03.050

Grain Boundary Engineering for Structure Materials of Nuclear Reactors

L. Tan [1,*], T.R. Allen [2], J.T. Busby [1]

[1] Materials Science and Technology Division, Oak Ridge National Laboratory

[2] Department of Engineering Physics, University of Wisconsin-Madison

[*] Corresponding author address: One Bethel Valley Road, P.O. Box 2008, MS-6151, Oak Ridge, TN 37831; Phone: 865-574-4628; E-mail: tanl@ornl.gov (L. Tan)

Abstract

Grain boundary engineering (GBE), primarily implemented by thermomechanical processing, is an effective and economical method of enhancing the properties of polycrystalline materials. Among the factors affecting grain boundary character distribution, literature data showed definitive effect of grain size and texture. GBE is more effective for austenitic stainless steels and Ni-base alloys compared to other structural materials of nuclear reactors, such as refractory metals, ferritic and ferritic-martensitic steels, and Zr alloys. GBE has shown beneficial effects on improving the strength, creep strength, and resistance to stress corrosion cracking and oxidation of austenitic stainless steels and Ni-base alloys.

Keywords: strength, stress corrosion cracking, oxidation, grain boundary, grain size

1. Introduction

Since the introduction of the grain boundary engineering (GBE) concept in the early 1980s, GBE has been investigated on a variety of polycrystalline metals and alloys to improve their properties, such as strength [1], ductility [2], creep [3], weldability [4], and stress corrosion cracking (SCC) and intergranular damage resistance [5,6]. Grain boundary character distribution (GBCD) and grain boundary (GB) connectivity have shown a close relationship with these material properties. The coincidence site lattice (CSL) model is employed to describe GBCD by classifying grain boundaries (GBs) as low-Σ CSL boundaries (CSLBs, Σ = 1-29) and general boundaries including high-Σ CSLBs (Σ > 29) and random boundaries. The Σ is the reciprocal density of coincident sites at the GB between two adjoining grains. Among the low-Σ CSLBs, Σ3 and Σ1 are usually the dominant boundaries. As a result of crystallographic constraints, GB connectivity is nonrandom, which describes the configurations of triple junctions, where 3 GBs come together, in a two-dimensional microstructure. (Triple junctions in a two-dimensional microstructure and quadruple nodes in a three-dimensional microstructure are topologically identical [7].) There are four types of triple junctions that can occur in a material, i.e., 0 low-Σ CSLB, 1 low-Σ CSLB, 2 low-Σ CSLBs, and 3 low-Σ CSLBs coming together. GB connectivity, being often simulated with percolation theory, quantitatively evaluates the frequency of resistant triple junctions that have more low-Σ CSLBs coming together. The two parameters, low-Σ CSLBs and GB connectivity, can be efficiently characterized by electron backscatter diffraction (EBSD), often called orientation imaging microscopy (OIM). Among the five macroscopic parameters used to distinguish each GB [8], GB plane also showed some effects on the properties of materials [9]. However, the two critical parameters are generally the most efficient and effective ones correlated with properties.

Low-Σ CSLBs including low-angle boundaries (or Σ1) are often called "special" boundaries due to their "special" properties compared to general boundaries, e.g., low boundary energies, resulting in less impurity segregation, higher resistance to oxidation and crack nucleation and propagation. Among the low-Σ CSLBs, the contribution of Σ3 boundaries to property improvement was observed to be the most prominent [10,11]. This is because the energy of Σ3 boundaries is extremely low, typically about 1/50 of a general boundary [8]. However, having a higher fraction of low-Σ CSLBs is not the only factor to produce enhanced properties. It has been observed that an increase in the frequency of resistant triple junctions enhances corrosion resistance of polycrystalline austenitic stainless steel even if the GBCD is the same [12]. The purpose of GBE is to improve materials' properties via increasing the fraction of low-Σ CSLBs, primarily Σ3 boundaries, and disrupting the connectivity of general boundaries (namely increasing the frequency of resistant triple junctions).

Thermomechanical processing (TMP), using single or multiple step(s) of deformation and subsequent annealing, has been the most popular approach applied for GBE. Some researchers [13,14,15,16,17] have compared the effect of different TMP parameters, such as deformation level, annealing temperature, and the number of steps, on GBE. Although a universal TMP is not available due to the distinctions between materials, multiple-step TMP is more favorable for a majority of materials with twinning-induced GBE. Other approaches for GBE, such as the application of magnetic field [18] and unidirectional solidification or annealing [19], have been developed for some specific materials, such as Fe-base alloys, steels, Al alloys, and Ni_3Al.

2. Factors affecting GBCD

GBCD may be influenced by many factors. For example, alloying elements may significantly change the diffusion and new-phase formation in materials, constraining the migration of GBs. Belluz and Aust [20] observed a significant increase in the fraction of low-Σ CSLBs by a small amount of Sn addition in high-purity Al but no effect of Ti addition. Experiments as well as theoretical studies have shown relatively definitive effects of grain size and texture on GBCD [21-31].

Watanabe [21] summarized the relationship between GBCD and grain size ranging from ~2 μm to ~2 mm for body-centered cubic (bcc) and face-centered cubic (fcc) metals and alloys having high stacking fault energies (SFEs), including Fe, Fe-9.45Co, Fe-3Si, Fe-1.69Sn, W, Mo, and Al. As shown in Fig. 1, these data approximately followed the same trend with an inverse dependence on grain size and the fraction of low-Σ CSLBs. As shown in Fig. 1, however, the data of stainless steel (SS) 304 [22], a fcc alloy with low SFEs, suggest a positive relationship between grain size and the fraction of low-Σ CSLBs. This is believed to be a result of the low SFEs favoring the formation of multiple twinning (Σ3, Σ9 and Σ27) during grain growth. The positive relationship was also observed in ultrafine-grained Ni (~0.1-0.5 μm), as shown in Fig. 1, which was fabricated by either severe plastic deformation [23,24] or electrodeposition [25]. Additionally, it is interesting to see that the limited data of the rapidly solidified and annealed Fe-6.5Si ribbons [26] suggest a positive relationship within the grain size range of ~40-600 μm. The mechanism for the change from an inverse relationship of the Fe alloys to a positive relationship of the Fe-6.5Si ribbons is not clear yet. According to these data, it may be deduced that a positive relationship between grain size and the fraction of low-Σ CSLBs is likely to be observed in fcc materials with low SFEs, which facilitate the increase of Σ3 boundaries, and nonequilibrium-fabricated materials. However, an inverse relationship is likely to be observed in

bcc and fcc materials with high SFEs, which need smaller grains possessing a larger population of GBs to increase the conversion opportunity from general boundaries to low-Σ CSLBs. More experimental data are needed to confirm the relationships for the different types of materials.

It has been found that crystalline texture can strongly affect GB misorientation, leading to the change of CSLBs distributions. For example, (111) Σ3 (i.e., 60° rotation around <111> axis) boundaries can easily form in grains with {111} texture because of the crystallographic constraints. The dependence of the formation readiness of CSLBs with specific Σ values on the specific fiber textures and their intensities has been illustrated by modeling [27,28] and experiments in a variety of cubic materials, e.g., SS316 [29] and ferritic 11 wt.%Cr alloys [30]. Moreover, such a relationship between low-Σ CSLBs and textures was observed in nonequilibrium-fabricated materials, e.g. Fe-6.5Si ribbons [26] and equal-channel angular extruded steels [31]. The favored low-Σ CSLBs by {100}, {110} and {111} fiber textures are summarized in Table 1. It is clear that the rotation axes of the respective low-Σ CSLBs are consistent with the corresponding textures. The fraction of low-Σ CSLBs systematically increases with the increasing sharpness of the specific textures.

3. GBE for structural materials of nuclear reactors

Organizing by crystal structure, structural materials of nuclear reactors can be categorized as fcc materials such as austenitic stainless steels and Ni-base alloys, bcc materials such as ferritic and ferritic-martensitic steels and refractory metal alloys, and hexagonal close-packed (hcp) materials such as Zr-base alloys. Some representative materials are discussed in Ref. [32]. GBE has been successfully employed to many austenitic stainless steels and Ni-base alloys due to their

low SFEs favoring the formation of twins introduced during TMP. Compared to the fcc alloys with low SFEs, GBE is difficult to implement in bcc metals and alloys that generally have high SFEs. Ferritic steels and refractory alloys may be able to be optimized by GBE with grain refinement as suggested in Fig. 1, with specific texture development, or using special approaches like magnetic annealing as suggested by a few successful examples [33,34]. However, the implementation of GBE on ferritic-martensitic steels is expected to be extremely difficult due to their complex microstructures with a high density of precipitates pinned on the dense martensitic packets and laths as well as prior-austenite boundaries, all of which prevent the migration and reaction of these boundaries.

Of the three crystal structures, the hcp structure is the most likely to twin during deformation due to its limited active slip systems. For example, twin density was increased to 45 areal% in a commercially pure Zr by means of TMP [35]. However, GBE is expected to be impractical on hcp metals and alloys. Compared to cubic metals, the CSLBs are meaningless in hcp metals because exact CSLs in hcp crystals depend on the (c/a) ratio of the lattice parameters except for rotations about the [0001] axis [36]. Furthermore, the temperature-dependent anisotropic thermal expansion affects the (c/a) ratio, leading to the uncertainty of exact CSLs. Consequently, the GB energy cusps existing at specific misorientations, e.g., (11-22) boundary at symmetrical [1-100] tilt boundaries [36], will be altered. Compared to cubic metals, the energy of high-angle boundaries in hcp metals is insensitive to the misorientation angle, which was calculated using the Read-Shockley equation that is dependent only on the misorientation angle obtained by geometric considerations rather than the atomic structure of the GBs [37].

Several examples of austenitic stainless steels and Ni-base alloys from the literature and the work of the authors are presented below, demonstrating the beneficial effects of GBE on improving the properties of the structural materials for nuclear reactors.

3.1. Strength

GBE increases the population of low energy boundaries (i.e., low-Σ CSLBs) and disrupts the connectivity of general boundaries, which mitigate intergranular fracture in polycrystalline materials. Figure 2(a) schematically illustrates a cracking path. The change of the fracture mode from intergranular to transgranular increases the strength of the materials [2]. GBE-induced strengthening was observed in Alloys 617 [38] and 800H [39,40]. The GBE treatments did not significantly alter the grain size of the alloys. GBE-induced strengthening, which was assessed by impact tests and tensile tests [40,41], was evidenced in an Alloy 800H subjected to a specific TMP [41], showing primary transgranular fracture. Figure 2(b) shows the yield and ultimate stresses of the as-received and GBE-treated Alloy 800H samples after ~1.4 dpa neutron irradiation at 580°C and 660°C. The results of the non-irradiated as-received samples are included for comparison. The irradiations produced radiation hardening (increase in yield strength) as compared to the results of the as-received samples. Significant increases in yield and ultimate stresses were observed in the GBE-treated samples. It's not possible to directly differentiate the GBE strengthening from the radiation hardening in the irradiated GBE-treated samples due to the lack of the tensile results of non-irradiated GBE-treated samples. However, the stress increases, compared to the irradiated as-received samples, can be primarily regarded as the result of the GBE treatment if the radiation hardening level is assumed to be the same in both the as-received and GBE-treated samples. Thus, the GBE-treatment increased the yield stresses up to 49% and 14% at 580°C and 660°C, respectively. Such pronounced strengthening generated

by the GBE treatment did not significantly impair the material ductility, e.g., 8.5% and 3.8% reduction in total elongation at 580°C and 660°C, respectively [39,40]. Detailed microstructure analysis of the non-irradiated samples indicated that the TMP also introduced dispersed precipitates at nanoscales [42]. Based on the classic precipitate strengthening mechanism, however, the amount of strength increase induced by these nano-precipitates only accounts ~9% of the increase from the as-received (solution-annealed) samples at 580°C – 660°C [42], which suggests that the GBE may have played a major effect on the strengthening.

$M_{23}C_6$ carbides (M is Cr- and/or Mo-rich) are common precipitates in both austenitic stainless steels and Ni-base alloys, which are detrimental to creep strength due to their preferential cavitation [43]. It was observed that this type of carbide dissolves and re-precipitates on boundaries in tension during creep at high temperatures [44]. GB character was found to be an important factor affecting the geometry and distribution of the carbides [42]. Low-Σ CSLBs showed significantly lower probability of associating with void development compared to general boundaries in Alloy 617 subjected to creep at 900−1000°C [45]. Figure 3 shows an EBSD map of Alloy 800H tested at 850°C. The image quality background distinguishes the general boundaries (G) and Σ3 boundaries and some defects inside grains. Large black voids exist at the general boundaries. The overlapped strain distribution highlights strains intensified around the voids and the general boundaries. Furthermore, consistent experimental observations and multi-scale simulations, using rate equations together with molecular dynamics and statics calculations, indicated that radiation-induced segregation can be suppressed by low-Σ CSLBs, especially for Σ3 and Σ9 boundaries, in austenitic stainless steels [46], leading to altered distribution of precipitates. Thus, a higher fraction of low-Σ CSLBs is expected to enhance creep strength.

3.2. SCC

Intergranular SCC (IGSCC) and irradiation-assisted SCC (IASCC) are typical modes of environmental degradation in nuclear power plants. Figure 4 exhibits an IGSCC example illustrating the effect of the fraction of low-Σ CSLBs on the number fraction of cracked boundaries in 304 and 316L stainless steels and the length fraction of cracked boundaries in Alloys 600 and 690 [47,48,49]. This figure only intends to compare the same material under different conditions (i.e., with different low-Σ CSLBs) rather than to compare different materials because the tests were not performed at the same condition. The crack length was defined as the total length of a continuous crack that often extended across several boundaries on the gage surface of the tested specimen. The crack boundaries were characterized and measured using secondary electron images. Figure 4 indicates that the increased fraction of low-Σ CSLBs led to the reduction of the number/length fraction of cracked boundaries in these materials. The available data suggest that the greater increase in the fraction of low-Σ CSLBs, $(F_{GBE} - F_{AR})/F_{AR}$, led to the more significant reduction in the fraction of the cracked boundaries, $(C_{GBE} - C_{AR})/C_{AR}$. Furthermore, the lower applied strain levels showed a greater reduction in the fraction of cracked boundaries. The increased resistance to IGSCC of the GBE-treated samples is attributable to the low energy nature of the low-Σ CSLBs, which also substantially decreased the intergranular crack-propagation velocity [50].

Unlike the prevalent beneficial effect of GBE on IGSCC, a recent crack growth test on 304 and 316 stainless steels in simulated boiling water reactor (BWR) water environments under neutron irradiation showed somewhat higher susceptibility to IASCC and considerably greater crack growth rates for GBE-treated samples [51]. Microstructure examination of the nonirradiated samples suggested that the beneficial effects of low-Σ CSLBs may have been

overwhelmed by detrimental effects of the significant amount of brittle precipitates and grain size enlargement introduced by the GBE treatments. This study suggests that TMP is systematic microstructure engineering for complex alloys, which alters not only GBCD but also precipitates. Special attention must be paid to the selection of TMP parameters to obtain optimum microstructures.

3.3. Oxidation

Supercritical water (SCW) tests at 500 and 600 °C showed significant difference in corrosion behavior between the as-received and the GBE-treated samples of Alloys 800H and 617 [39,52,53,54,55]. Figure 5 shows an example of Alloy 800H samples exposed to SCW at 600 °C. Significant oxide exfoliation was observed on the as-received sample (~51% low-Σ CSLBs) with most of the exfoliation occurring at the magnetite-spinel interface and some at the hematite-magnetite interface. In contrast, the oxide scale on the GBE-treated sample (~75% low-Σ CSLBs) maintained good integrity with a continuous hematite layer at the surface. Despite the presence of the same oxide components, i.e., hematite, magnetite, and spinel from surface to metallic matrix, on the as-received and the GBE-treated samples, the raised amount of hematite on the GBE-treated samples introduced hematite-spinel interface and reduced hematite-magnetite and magnetite-spinel interfaces, leading to the integrity of the oxide scale on the GBE-treated sample because of the smaller thermal expansion mismatch at the hematite-spinel interface compared to the other two types of interfaces [39,52]. In addition to the benefit of the optimized GBCD, it is believed that the change from tangled dislocation networks in the as-received samples to discrete dislocations in the GBE-treated samples has played an important role on the microstructural change of the oxide scale [42]. The increased fraction of low-Σ CSLBs and reduced dislocation networks in the GBE-treated samples may have significantly reduced the outward transport of Fe,

resulting in less Fe supplied to the GBE-treated sample surface compared to that on the as-received sample. The reduced Fe resulted in a relatively higher oxygen activity favoring hematite formation.

Figure 6 shows the weight change of Alloys 800H and 617 samples cyclically exposed to air at 850 and 1000 °C, respectively. Each cycle was composed of putting the samples in a furnace at the designated temperatures for a heating period of 24 h and followed by pulling the samples out for air cooling to room temperature for ~15 min to measure the weight changes. Thus, each data point in Fig. 6 corresponds to one cycle. Both the as-received and the GBE-treated Alloy 800H samples showed small weight gains within a short period of exposure at 850 °C, and then changed to weight losses. However, the weight losses of the GBE-treated sample were significantly smaller than that of the as-received sample. Better oxide scale integrity was observed on the GBE-treated samples [53]. In comparison, the Alloy 617 samples showed weight gains during the exposure at 1000 °C. The weight gains of the GBE-treated sample were about half of the as-received sample. The cross-sectional morphologies of the oxide scales formed on the Alloy 617 samples are shown in Fig. 7 with the as-received sample on the upper-left and the GBE-treated sample on the lower right. A significant amount of GB oxidation (either discrete or continuous) and large voids were observed in the as-received sample (with ~53% low-Σ CSLBs) beneath the oxide scale as deep as ~50 μm. In contrast, only a few discrete areas of GB oxidation and small voids were observed in the GBE-treated sample (with ~79% low-Σ CSLBs) beneath the oxide scale as deep as ~30 μm. Analytical microstructure analysis indicated that the GBE-treated samples were completely covered with Cr_2O_3 with some TiO_2 at surface. In contrast, the oxide scale on the as-received samples was primarily composed of Cr2O3 mixed with some Ni-rich spinel and a few TiO_2. The disconnected general boundaries as well as the

significantly reduced amount of general boundaries may have played an important role on the supply of preferential oxidation elements like Cr and Ti. Further investigations are needed to obtain explicit mechanisms that resulted in the significant differences between the GBE-treated and as-received samples.

4. Summary

Grain boundary engineering (GBE) is an effective and economical method of enhancing material properties. Despite many special approaches having been developed to create favorable grain boundary character distributions (GBCD), thermomechanical processing (TMP) is the most popular approach used for GBE. Substantive evidence indicates relatively definitive relationships between GBCD and grain size and texture.

GBE by means of specific TMP is useful with structural materials for nuclear applications, such as austenitic stainless steels and Ni-base alloys, which can effectively enhance materials' strength and resistance to SCC and oxidation. The application of GBE to other structural materials, such as refractory metals, ferritic and ferritic-martensitic steels, is not as effective as to austenitic steels and Ni-base alloys. Nonetheless, optimized microstructures are expected to be obtainable by employing special approaches with controlled grain size and texture. Reliable property improvements induced by GBE have not been achieved in Zr alloys due to their hcp structure with an anisotropic thermal expansion of (c/a) lattice parameter ratio.

Acknowledgements

This research was supported in part by an appointment to the U.S. Department of Energy (DOE) Higher Education Research Experiences (HERE) for Faculty at the Oak Ridge National Laboratory (ORNL) administered by the Oak Ridge Institute for Science and Education. The authors would like to express special thanks to Drs. R.K. Nanstad and Y. Yamamoto for their technical reviews and thoughtful comments.

References

[1] U. Erb, P. Lin, S. Kim, K.T. Aust, F. Gonzalez, G. Palumbo, in: T.S. Srivatsan, R.A. Varin (Eds.), Proceedings of the 10th International Symposium on Processing and Fabrication of Advanced Materials, Indianapolis, IN, USA, 5-8 November, 2001, p. 3-18.
[2] T. Watanabe, S. Tsurekawa, Acta Mater. 47 (1999) 4171-4185.
[3] D.S. Lee, H.S. Ryoo, S.K. Hwang, Mater. Sci. Eng. A 354 (2003) 106-111.
[4] E.M. Lehockey, G. Palumbo, P. Lin, Metall. Mater. Trans. A 29 (1998) 2069-2079.
[5] M. Shimada, H. Kokawa, Z.J. Wang, Y.S. Sato, I. Karibe, Acta Mater. 50 (2002) 2331-2341.
[6] V.Y. Gertsman, K. Tangri, Modelling of intergranular damage propagation, Acta Mater 45 (1997) 4107-4116.
[7] M. Frary, Determination of three-dimensional grain boundary connectivity from two-dimensional microstructures, Scripta Materialia 57 (2007) 205-208.
[8] V. Randle, The Role of the Coincidence Site Lattice in Grain Boundary Engineering, The Institute of Materials, London, 1996.
[9] V. Randle, 'Special' boundaries and grain boundary plane engineering, Scripta Mater. 54 (2006) 1011.
[10] Y. Pan, B.L. Adams, T. Olson, N. Panayotou, Acta Mater. 44 (1996) 4685.
[11] V.Y. Gertsman, S.M. Bruemmer, Acta Mater. 49 (2001) 1589.
[12] S. Tsurekawa, S. Nakamichi, T. Watanabe, Correlation of grain boundary connectivity with grain boundary character distribution in austenitic stainless steel, Acta Mater. 54 (2006) 3617-3626.
[13] V. Randle, Mechanism of twinning-induced grain boundary engineering in low-stacking-fault energy materials, Acta Mater 47 (1999) 4187-4196.
[14] G. Owen, V. Randle, One the role of iterative processing in grain boundary engineering, Scripta Mater 55 (2006) 959-962.
[15] V. Randle, M. Coleman, A study of low-strain and medium-strain grain boundary engineering, Acta Mater 57 (2009) 3410-3421.
[16] V. Randle, R. Jones, Grain boundary plane distributions and single-step versus multiple-step grain boundary engineering, Mater Sci Eng A 524 (2009) 134-142.
[17] S.M. Schlegel, S. Hopkins, M. Frary, Effect of grain boundary engineering on microstructural stability during annealing, Scripta Mater 61 (2009) 88-91.

[18] T. Watanabe, High temperature magnetic strengthening in iron-based alloys: magnetic effects on deformation and fracture, revisited, Inter J Mater Res 100 (2009) 614-624.
[19] T. Hirano, Improvement of room-temperature ductility of stoichiometric Ni_3Al by unidirectional solidification, Acta Metall Mater 38 (1990) 2667-2671.
[20] R.V. Belluz, K.T. Aust, Effect of solutes on preferred orientation in high-purity aluminum, Met Trans 6 (1975) 219-220.
[21] T. Watanabe, Grain-boundary design for advanced materials on the basis of the relationship between texture and grain-boundary-character-distribution (GBCD), Textures and Microstructures 20 (1993) 195-216.
[22] S. Tsurekawa, S. Nakamichi, T. Watanabe, Correlation of grain boundary connectivity with grain boundary character distribution in austenitic stainless steel, Acta Mater 54 (2006) 3617-3626.
[23] A.P. Zhilyaev, B.-K. Kim, J.A. Szpunar, M.D. Baró, T.G. Langdon, The microstructural characteristics of ultrafine-grained nickel, Mater Sci Eng A 391 (2005) 377-389.
[24] K.S. Raju, M.G. Krishna, K.A. Padmanabhan, K. Muraleedharan, N.P. Gurao, G. Wilde, Grain size and grain boundary character distribution in ultra-fine grained (ECAP) nickel, Mater Sci Eng A 491 (2008) 1-7.
[25] K. Harada, S. Tsurekawa, T. Watanabe, G. Palumbo, Enhancement of homogeneity of grain boundary microstructure by magnetic annealing of electrodeposited nanocrystalline nickel, Scripta Mater 49 (2003) 367-372.
[26] T. Watanabe, H. Fujii, H. Oikawa, J.I. Arai, Grain boundaries in rapidly solidified and annealed Fe-6.5mass% Si polycrystalline ribbons with high ductility, Acta Metall 37 (1989) 941-952.
[27] A. Garbacz, M.W. Grabski, The relationship between texture and CSL boundaries distribution in polycrystalline materials .2. analysis of the relationship between texture and coincidence grain-boundary distribution, Acta Metall Mater 41 (1993) 475-483.
[28] R.E. García, M.D. Vaudin, Correlations between the crystallographic texture and grain boundary character in polycrystalline materials, Acta Mater 55 (2007) 5728-5735.
[29] K.J. Kurzydlowski, B. Ralph, J.J. Bucki, A. Garbacz, The grain boundary character distribution effect on the flow stress of polycrystals: the influence of crystal lattice texture, Mater Sci Eng A 205 (1996) 127-132.
[30] H. Yan, H. Bi, X. Li, Z. Xu, Microstructure, texture and grain boundaries character distribution evolution of ferritic stainless steel during rolling process, J Mater Process Tech 209 (2009) 2627-2631.
[31] A. Bhowmik, S. Biswas, S. Suwas, R.K. Ray, D. Bhattacharjee, Evolution of grain-boundary microstructure and texture in interstitial-free steel processed by equal-channel angular extrusion, Metall Mater Trans A 40 (2009) 2729-2742.
[32] T.R. Allen, K. Sridharan, L. Tan, W.E. Windes, J.I. Cole, D.C. Crawford, G.S. Was, Materials challenges for generation IV nuclear energy systems, Nucl Tech 162 (2008) 342-357.
[33] T. Watanabe, Y. Suzuki, S. Tanii, H. Oikawa, The effects of magnetic annealing on recrystallization and grain-boundary character distribution (GBCD) in iron-cobalt alloy polycrystals, Phil. Mag. Letters 62 (1990) 9.
[34] S. Tsurekawa, T. Watanabe, Grain boundary microstructure dependent – intergranular fracture in polycrystalline molybdenum, Mat. Res. Soc. Symp. Proc. 586 (2000) 237.

[35] J.H. Chung, Development of thermomechanical processing method to enhance twinning in commercially pure Zr, Scripta Mater 61 (2009) 161-164.
[36] M.S. Wu, A.A. Nazarov, K. Zhou, Misorientation dependence of the energy of [1-100] symmetrical tilt boundaries in hcp metals: prediction by the disclination-structural unit model, Phil. Mag. 84 (2004) 785-806.
[37] S.H. Yu, Y.B. Chun, S.K. Hwang, D.H. Shin, Texture development and Monte-Carlo simulation of microstructure evolution in pure Zr grain-refined by equal channel angular pressing, Phil. Mag. 85 (2005) 345-371.
[38] L. Tan, K. Sridharan, T.R. Allen, Effect of thermomechanical processing on grain boundary character distribution of a Ni-based superalloy, J Nucl Mater 371 (2007) 171-175.
[39] L. Tan, K. Sridharan, T.R. Allen, R.K. Nanstad, D.A. McClintock, Microstructure tailoring for property improvements by grain boundary engineering, J. Nucl. Mater. 374 (2008) 270-280.
[40] R.K. Nanstad, D.A. McClintock, D.T. Hoelzer, L. Tan, T.R. Allen, High temperature irradiation effects in selected Generation IV structural alloys, J Nucl Mater 392 (2009) 331-340.
[41] L. Tan, T.R. Allen, An EBSD study of grain boundary engineered INCOLOY alloy 800H, Metall Mater Trans A 36 (2005) 1921-1925.
[42] L. Tan, L. Rakotojaona, T.R. Allen, R.K. Nanstad, J.T. Busby, Microstructure optimization of Incoloy austenitic alloy 800H (Fe-21Cr-32Ni), Mater. Sci. Eng. A 528 (2011) 2755-2761.
[43] K.S. Min, S.C. Lee, S.W. Nam, Effects of TiC and $Cr_{23}C_6$ carbides on creep-fatigue properties in AISI 321 stainless steel, Materials Transactions 43 (2002) 2808-2812.
[44] S. Schlegel, S. Hopkins, E. Young, J. Cole, T. Lillo, M. Frary, Precipitate redistribution during creep of alloy 617, Metall Mater Trans A 40 (2009) 2812-2823.
[45] T. Lillo, J. Cole, M. Frary, S. Schlegel, Influence of grain boundary character on creep void formation in alloy 617, Metall Mater Trans A 40 (2009) 2803-2811.
[46] N. Sakaguchi, S. Watanabe, H. Takahashi, R.G. Faulkner, A multi-scale approach to radiation-induced segregation at various grain boundaries, J Nucl Mater 329-333 (2004) 1166-1169.
[47] V.Y. Gertsman, S.M. Bruemmer, study of grain boundary character along intergranular stress corrosion crack paths in austenitic alloys, Acta Mater 49 (2001) 1589-1598.
[48] S.M. Bruemmer, Linking grain boundary structure and composition to intergranular stress corrosion cracking of austenitic stainless steels, Mat Res Soc Symp Proc 819 (2004) N2.2.1.
[49] E.A. West, G.S. Was, IGSCC of grain boundary engineered 316L and 690 in supercritical water, J Nucl Mater 392 (2009) 264-271.
[50] U. Krupp, Improving the resistance to intergranular cracking and corrosion at elevated temperatures by grain-boundary-engineering-type processing, J Mater Sci 43 (2008) 3908-3916.
[51] Y. Chen, O.K. Chopra, Y. Yang, W.J. Shack, B. Alexandereanu, E.E. Gruber, A.S. Rao, Crack growth rates and fracture toughness of neutron irradiated grain-boundary-engineered austenitic stainless steels, The 14th International Conference on Environmental Degradation of Materials in Nuclear Power Systems, Virginia Beach, VA, USA, August 23-27, 2009.
[52] L. Tan, K. Sridharan, T.R. Allen, The effect of grain boundary engineering on oxidation behavior of INCOLOY alloy 800H in supercritical water, J Nucl Mater 348 (2006) 263-271.
[53] L. Tan, K. Sridharan, T.R. Allen, Altering corrosion response via grain boundary engineering, Mater Sci Forum 595-598 (2008) 409-418.

[54] G.S. Was, P. Ampornrat, G. Gupta, S. Teysseyre, E.A. West, T.R. Allen, K. Sridharan, L. Tan, Y. Chen, X. Ren, C. Pister, Corrosion and stress corrosion cracking in supercritical water, J Nucl Mater 371 (2007) 176-201.

[55] L. Tan, X. Ren, K. Sridharan, T.R. Allen, Corrosion behavior of Ni-based alloys exposed to supercritical water, Corros Sci 50 (2008) 3056-3062.

Captions of Figures and Tables

Fig. 1. Fraction of low-Σ CSLBs (Σ = 1-29) as a function of grain size in a variety of polycrystalline metals and alloys (adapted from Refs. 19-24).

Fig. 2. (a) Schematic illustration of enhanced fracture stress by changing fracture mode from intergranular to transgranular; (b) Yield and ultimate stresses of the as-received and GBE-treated Alloy 800H samples.

Fig. 3. EBSD maps with (a) image quality labeled with GB types (Σ3 and G – general) and (b) strain distribution (0°-5° kernel misorientation) of an Alloy 800H sample tested at 850°C.

Fig. 4. Fraction of cracked boundaries (*C*) as a function of the fraction of low-Σ CSLBs (*F*) in 304 and 316L stainless steels and Ni-base Alloys 600 and 690. Open and solid symbols denote the as-received and the GBE-treated conditions, respectively.

Fig. 5. Alloy 800H samples in the as-received (AR) and GBE-treated conditions exposed to SCW at 600°C for 1000 hours.

Fig. 6. Weight change of the Alloys 800H (850°C) and 617 (1000°C) samples in the as-received and the GBE-treated conditions exposed to air.

Fig. 7. Cross-section of the Alloy 617 samples in the as-received (AR) and the GBE-treated conditions exposed to air at 1000°C for 1008 hours.

Table 1. Fiber textures favored specific low-Σ CSLBs. The a and b after some of the Σ values denotes one of the variants of the specific low-Σ CSLB.

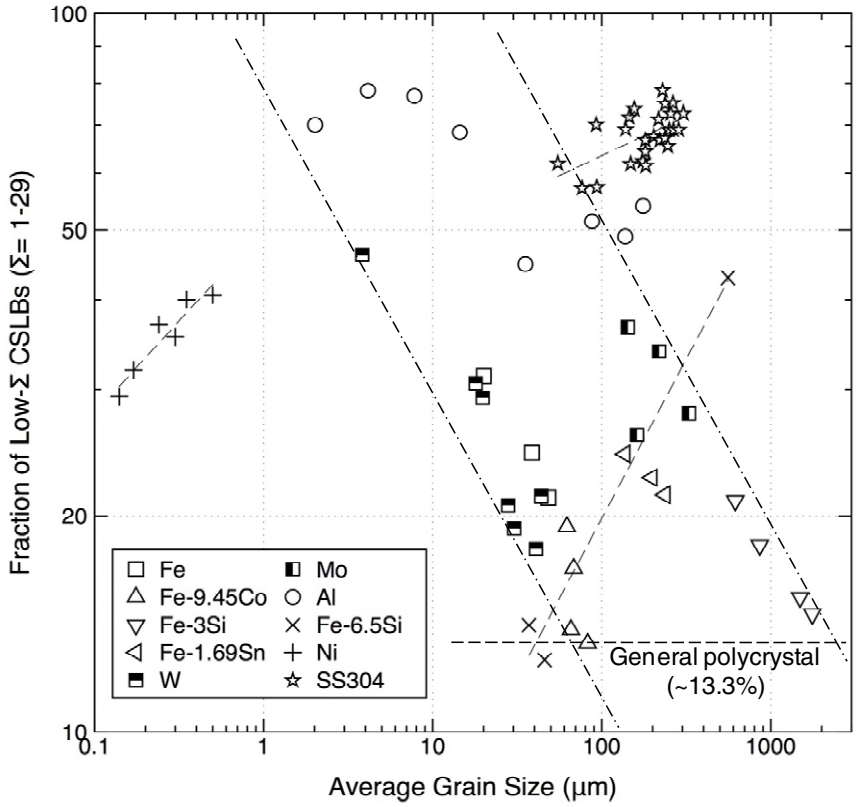

Fig. 1. Fraction of low-Σ CSLBs (Σ = 1-29) as a function of grain size in a variety of polycrystalline metals and alloys (adapted from Refs. 19-24).

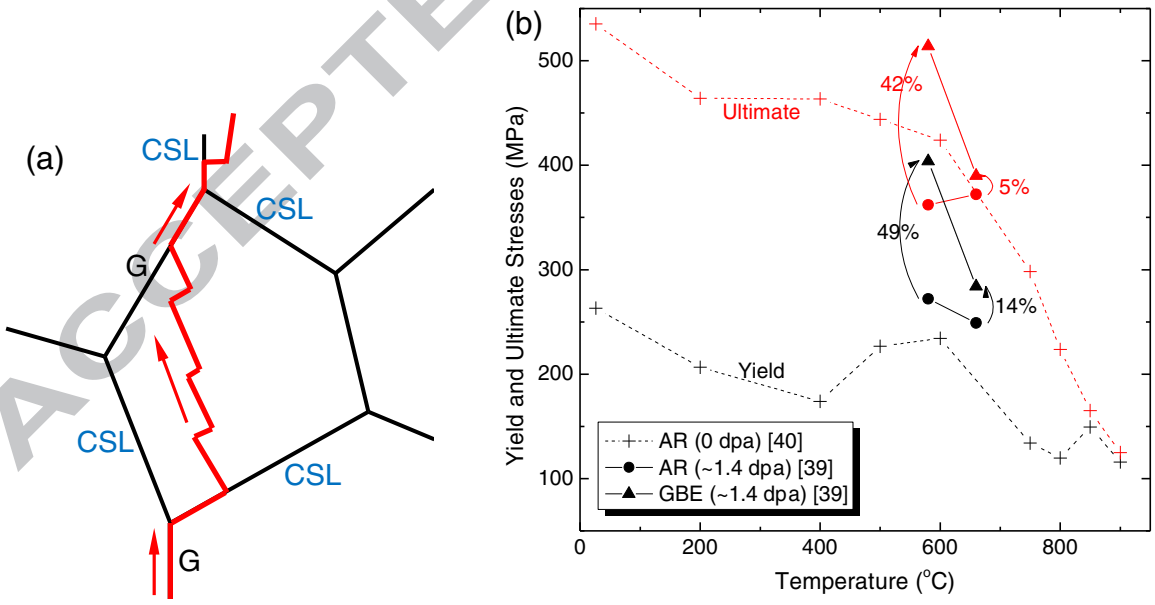

Fig. 2. (a) Schematic illustration of enhanced fracture stress by changing fracture mode from intergranular to transgranular; (b) Yield and ultimate stresses of the as-received and GBE-treated Alloy 800H samples.

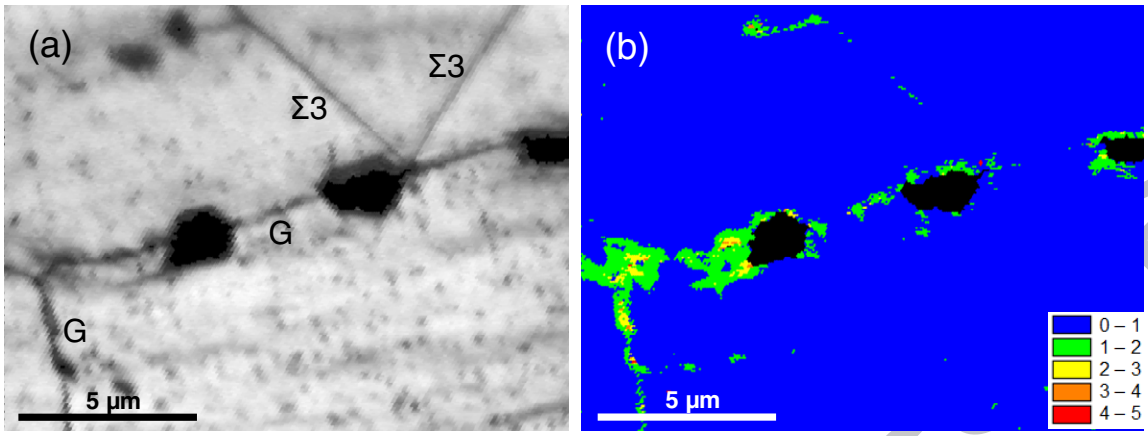

Fig. 3. EBSD maps with (a) image quality labeled with GB types (Σ3 and G – general) and (b) strain distribution (0°-5° kernel misorientation) of an Alloy 800H sample tested at 850°C.

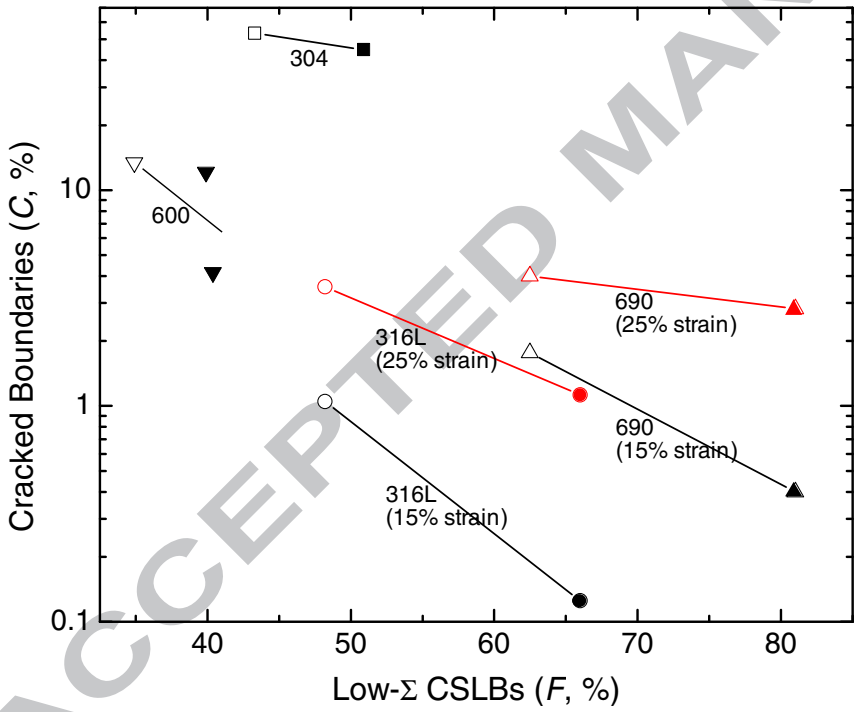

Fig. 4. Fraction of cracked boundaries (C) as a function of the fraction of low-Σ CSLBs (F) in 304 and 316L stainless steels and Ni-base Alloys 600 and 690. Open and solid symbols denote the as-received and the GBE-treated conditions, respectively.

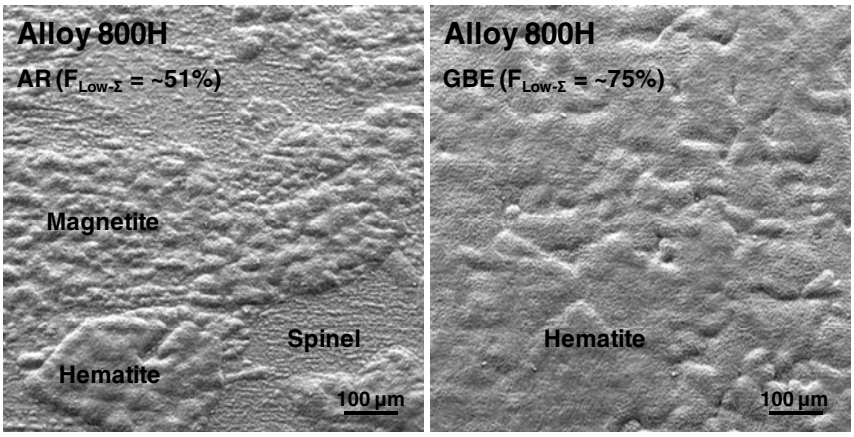

Fig. 5. Alloy 800H samples in the as-received (AR) and GBE-treated conditions exposed to SCW at 600°C for 1026 hours.

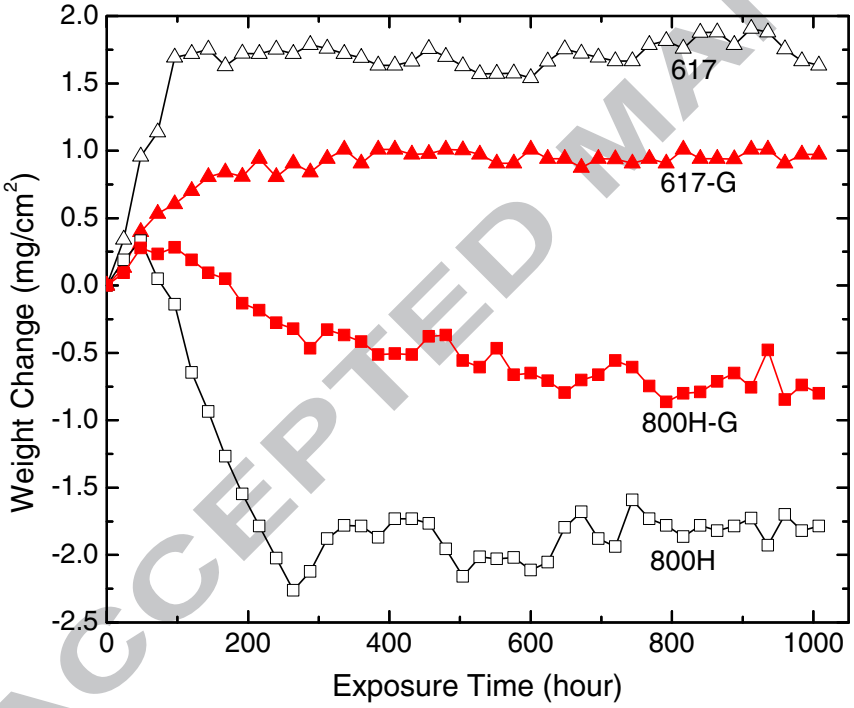

Fig. 6. Weight change of the Alloys 800H (850°C) and 617 (1000°C) samples in the as-received and the GBE-treated conditions exposed to air.

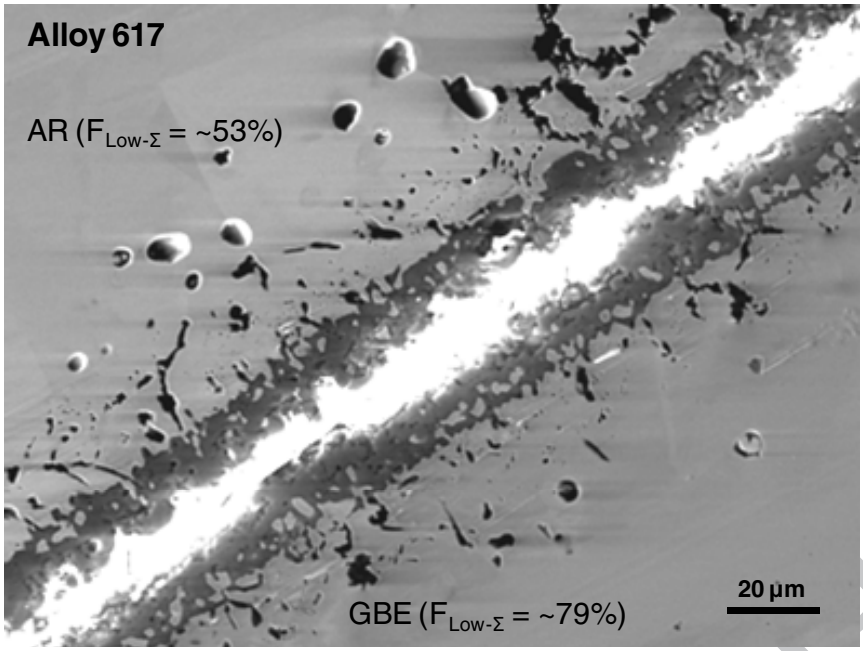

Fig. 7. Cross-section of the Alloy 617 samples in the as-received (AR) and the GBE-treated conditions exposed to air at 1000°C for 1008 hours.

Table 1. Fiber textures favored specific low-Σ CSLBs. The a and b after some of the Σ values denotes one of the variants of the specific low-Σ CSLB.

Texture	Low-Σ CSLBs (Σ = 1-29)
{100}	Σ1, 5, 13a, 17a, 25a, 29a (with <100> rotation axis)
{110}	Σ1, 3, 9, 11, 19a, 27a (with <110> rotation axis)
{111}	Σ1, 3, 7, 13b, 19b, 21a (with <111> rotation axis)